Case Studies in Thermal Engineering 8 (2016) 277–290

Contents lists available at ScienceDirect

Case Studies in Thermal Engineering

journal homepage: www.elsevier.com/locate/csite

The influence of turbulence models on the accuracy of CFD analysis of a reciprocating mechanism driven heat loop

Olubunmi Popoola*, Yiding Cao

Department of Mechanical and Materials Engineering, Florida International University, Miami, FL 33174, United States

ARTICLE INFO

Article history:
Received 17 August 2016
Received in revised form
28 August 2016
Accepted 30 August 2016

Keywords:
Heat loop
Reciprocating flow
Turbulence models

ABSTRACT

A bellows-type Reciprocating-Mechanism Driven Heat Loops (RMDHL) is a novel heat transfer device that could attain a high heat transfer rate through a reciprocating flow of the working fluid inside the heat transfer device. Although the device has been tested and validated experimentally, analytical or numerical study has not been undertaken to understand its working mechanism and provide guidance for the device design. In an effort to improve earlier numerical models of the RMDHL, different turbulence models for the RMDHL design have been studied and compared with prior experimental results to select the most suitable turbulence modeling techniques. The governing equations have been numerically solved using a CFD solver. For the three-dimensional fluid flow, several turbulence models have been studied for the RMDHL, including Standard, RNG, and Realizable k-ε Models, Standard and SST k-ω Models, Transition k -k_L-ω Model and the Transition SST Model. The results of the simulations have been analyzed and ranked using numerical model calibration template. It was found that the standard k-ω Models provided the least accurate results while the RNG-k-ε Model provided the most accurate predictions. It is expected that the results will help improve the accuracy of the work on the RMDHL modeling.

1. Introduction

Cao and Gao [1,2] conceived, designed and tested novel solenoid and bellows-type Reciprocating Mechanism Driven Heat Loops (RMDHL) or the reciprocating-flow heat loops, which attains a reciprocating flow of the working fluid inside the heat transfer device without requiring a reciprocating motion of the entire heat transfer device. The RMDHL, includes a hollow loop having an interior flow passage, an amount of working fluid filled within the loop, and a reciprocating driver. The heat loop has an evaporator section, a condenser section, and a liquid reservoir. The reciprocating driver is integrated with a liquid reservoir and facilitates a reciprocating flow of the working fluid within the heat loop, so that liquid is supplied from the condenser section to the evaporator section and a high heat transfer rate from the evaporator section to the condenser section is achieved. Temperature uniformity is also attained when the air is evacuated from the loop and the working fluid hermetically sealed within the loop is under a substantially saturated condition. Considering the advantages of coolant leakage free and the absence of cavitation problems for aerospace related applications, RMDHL could be an alternative to a conventional LCS for electronic cooling applications.

* Corresponding author.
E-mail address: opopo002@fiu.edu (O. Popoola).

http://dx.doi.org/10.1016/j.csite.2016.08.009

Nomenclature

A	Area [m^2]
C_p	Specific heat [J/kg K]
D_i	Inside tube diameter [m]
D_o	Tube outside diameter [m]
D_h	Hydraulic diameter [m]
H	Height of rectangular channel [m]
h	Heat-transfer coefficient [W/m^2 K]
k	Thermal conductivity [W/m^2K]
L	length
$\dot{m}$	Mass flow rate [kg/s]
n	Reciprocating pump stroke frequency cycles/s
Nu	Nusselt number: $h/(k/D_h)$
p	pressure [Pa]
$\dot{Q}$	Heat-transfer rate [W]
q	volume flow rate [m^3/s]
Re	Reynolds number: $(\rho VD)/\mu$
Re_ω	kinetic Reynolds number: $\frac{\omega x_{max}^2}{\nu}$ [m]
r	Tube inside radius [m]
S	Stroke [m]
T	Temperature [°C]
U	Overall heat-transfer coefficient [W/m^2 K]
t	time s

Greek letters

δ	Flow penetration
σ_T	Standard deviation
α	Surface effectiveness: $\sqrt{\frac{2\nu}{\omega}}$
μ	Dynamic viscosity [kg/ms]
ρ	Density [kg/m^3]
ω	pump frequency [rad/s]
τ	cycle period s
σ	Constant: $\frac{8}{\alpha^3}\sqrt{(\alpha - 2C_1)^2 + 4C_2^2}$

Subscript

ave	average value
c	condenser
e	evaporator
in	inlet
m	mean value
min	minimum value
max	maximum value
n	direction normal to the wall
p	pump piston
out	outlet
s	surface
t	tubing
w	wall

Superscript

=-	time-averaged quantity
→	vector

The types of flows that are typical of the RMDHL environment are characterized by unsteady (oscillatory flow and oscillatory pressure), 2-D/3-D (complex geometry), compressible (low Mach number), turbulent, and unsteady fluid flows as well as conduction and turbulent convection heat transfer. Other conditions include sudden changes in cross-section and isothermal and adiabatic boundary conditions [3–5]. As a result, understanding the heat transfer and pressure drop in the RMDHL under operating conditions will require accurate and robust Computational Fluid dynamics (CFD) and turbulence modeling capability is critical to the success of the CFD. It is understandable that turbulence is arguably the most challenging area in CFD. No single model or modeling approach can cover all types of turbulent flows; different types of turbulence models have been developed in the past decades [6–19]. Due to the lack of suitable correlations for oscillating flow conditions in the literature, correlations derived from steady state unidirectional flow assumptions are normally adopted for reciprocating flows [20–23].

Ahn and Ibrahim [11] conducted a two dimensional oscillating flow analysis simulating the gas flow inside Stirling heat exchangers for laminar and turbulent oscillating pipe flow. In the study, the performance evaluation of the K-ε model was made to explore its suitability to quasi-steady turbulent models in unsteady oscillating flow analysis. Ibrahim et al. [12] investigated the usefulness of a low Reynolds number version of k-ε to model the laminar, transitional, and turbulent flow in an oscillatory pipe flow between two parallel plates with a sudden change in cross section using. Su et al. [13] used the RANS method with Saffman's turbulence model to solve the time-dependent turbulent Navier–Stokes and energy equations for oscillating pipe flows. Wang and Lu [16] investigated oscillating turbulent channel flow with heat transfer using the large eddy simulation (LES) technique. The conclusion in all the works reviewed above is that the unidirectional flows models in some cases either does not include the effect of phase lag in heat transfer or does not reflect the influence of the oscillation frequency on the heat transfer and has sometimes proved to be inappropriate. Hence appropriate attention is required in selection of a suitable model.

In addition, majority of the investigations on the heat transfer in turbulent oscillating pipe flow has focused on the Stirling engines and Vuilleumier heat pumps type systems or high Reynolds number open channel applications. These systems typically use 2 cylinder volumes, which are located at different temperature levels. The volumes are periodically changed by pistons and displacers forcing the working fluid to oscillate within the process [21], in which it is convenient to the heat removal and heat addition to the working fluid in two separate analysis. Numerical modeling for the RMDHL requires that the heat removal and heat addition processes be coupled and the fluid flow and heat transfer must be simulated simultaneously. Depending on the Reynolds number the accuracy of the turbulence prediction can be affected

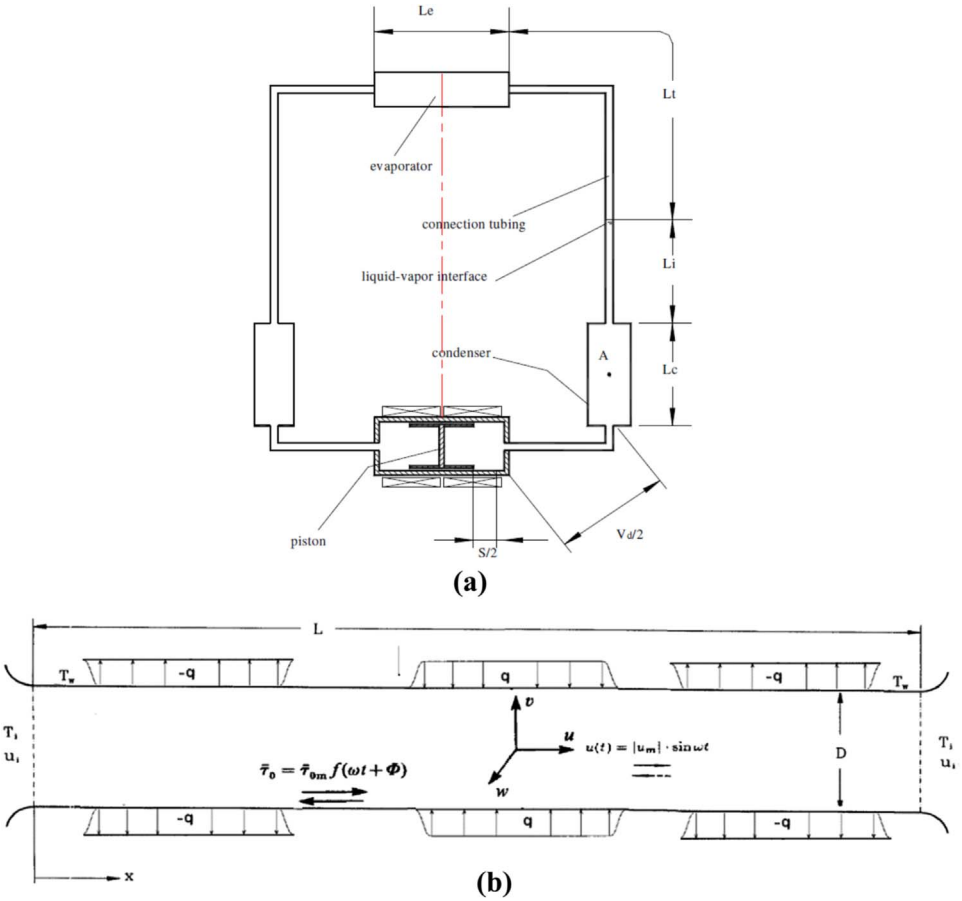

Fig. 1. The (a)geometric and (b)boundary conditions for this study.

based on heating or cooling. Fig. 1 is the schematic model for the RMDHL to be studied. The purpose of this study is to determine the most suitable turbulence model that produces the closest approximation to equilibrium conditions on the cold plate of the RMDHL.

Turbulence models can be classified as Zero, One, Two or Stress equation models based on the number of partial differential equations solved in addition to the mean flow equation [6]. The k-ε, k-k_L and the k-ω models belong to the two equation models. The standard and modified forms of the k-ε model is used in a majority of flows reported in literature. While the equally popular Transition k -k_L-ω and Transition SST are three equation models. This study will compare the accuracy of the predictions of the Standard k- ε Model, Renormalization-group (RNG) k- ε Model, Realizable k- ε Model, Standard k- ω, Shear-Stress Transport (SST) k- ω Model and Transition SST Model.

2. Design and construction of a concept-demonstration model of the bellows-type RMDHL

The prototype used for this investigation is shown in Fig. 1b, and the corresponding design, construction and specifications have been presented in [1,2]. One of the most important relations that describes the critical requirement for the operation of the heat loop is given as below:

$$A_p S \geq A_c L_C + 2A_t L_t + A_e L_e \tag{1}$$

The length and average interior cross-sectional area of the evaporator are denoted by L_e and A_e, respectively, the length and average interior cross-sectional area of the connection tubing between the evaporator and the condenser are L_t and A_t, the length and interior cross-sectional area of each condenser section are L_c and A_c. The piston cross-sectional area and reciprocating stroke are A_p and S, respectively. From the dimensions of the heat loop in Fig. 1b, the critical S was calculated as 7 cm and based on the ease of manufacturing, a value of 7.62 cm was used for the reciprocatory driver.

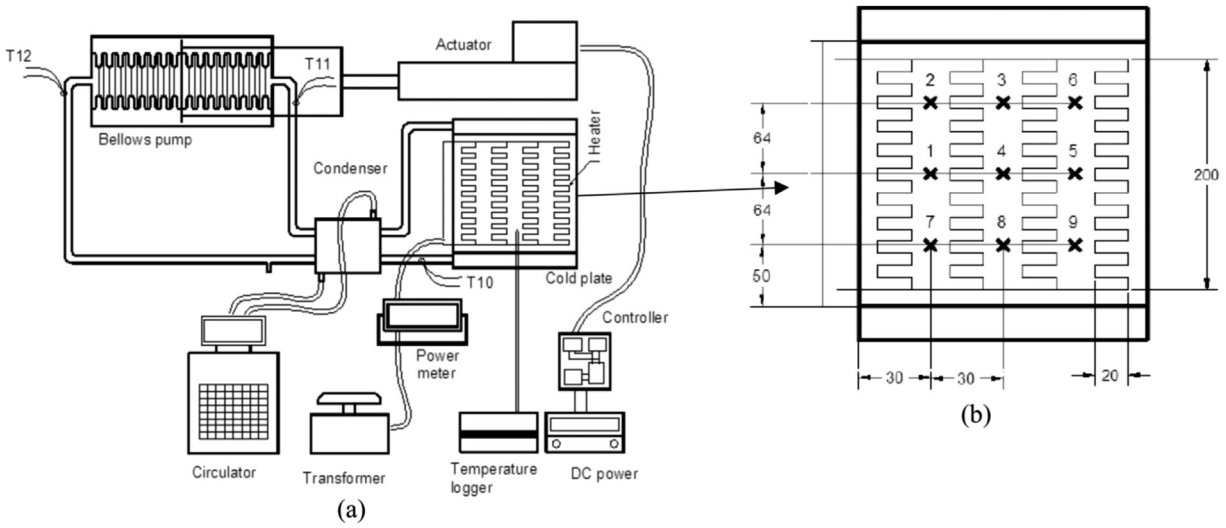

Fig. 2. Experimental setup: (a) overall arrangement and (b) thermocouple locations on the cold plate (size in mm).

3. Experimental study and test results of the bellows-type RMDHL demonstration model

The experimental setup for the bellows-type RMDHL demonstration model is similar to the setup shown in Fig. 2 [2,24]. The setup includes electric heaters for supplying heat to the cold plate of the heat loop, a DC power supply to the reciprocating driver, a control circuit board to control the reciprocating frequency of the driver, a constant temperature circulator to maintain a constant coolant inlet temperature of 10 °C to the condenser, which would also control the operating temperature level of the heat loop, a data acquisition system, and the fabricated heat loop. Eight Omega flexible heaters (four on each side of the cold plate) are clamped by two aluminum plates onto the cold plate with insulation layers sandwiched between the heaters and clamping plates. Each heater has a dimension of 2 cm by 12 cm and could provide a heat input up to 200 W.

Twelve thermocouples were placed at different locations of the heat loop. Nine of them (numbered as No. 1 through No. 9) are placed on the top surface of the cold plate at different locations for the study of temperature uniformity on the cold plate. Fig. 2b shows detailed locations of these thermocouples. One thermocouple is placed near the condenser and another two thermocouples are placed on two ends of the bellows pump to monitor the heat loop temperature distribution in addition to those on the cold plate. These three thermocouples are numbered, respectively, as T10, T11, and T12, as shown in Fig. 2b.

During the experimentation, the heat loss from the clamping plate to the ambient was amounted to be less than 1%. Therefore, the sources of the experimental uncertainty were primarily due to the instruments themselves. The scanning thermocouple thermometer has an accuracy of $\pm 0.1\%$ of reading ± 0.4 °C. The power meter has an accuracy of $\pm(1\%$ reading $+5$ digits). So the maximum uncertainty for the temperature and heat power measurements would be 1.0% and 2%, respectively.

4. Formulations of the numerical study

It should be pointed out that the RMDHL can be either a single-phase or two-phase loop. For the present single-phase application, a single-phase RMDHL is considered. The commercial ANSYS Fluent CFD code was employed for the numerical simulation. The first step of the model development is the generation of a 3D CAD model of the process by SolidWorks. Both the condenser and evaporator of the loops are enclosed with solid wall. The solid walls are aluminum and thermophysical properties are obtained from the fluent database. The working liquid in the loops is water. To simplify the numerical modeling an open loop configuration of the heat loop is modeled, as shown in Fig. 3c and d.

4.1. Inlet/outlet conditions specifications

The Open Loop Geometry configuration for numerical model of the RMDH loop and the mesh grid distribution for numerical simulations of the RMDH loop is shown in Fig. 3b. The displacement of the piston $x_p(t)$ with time is [25]:

$$x_p(t) = -\tfrac{1}{2}S - \tfrac{1}{2}S\cos(\omega t) \tag{2}$$

where ω is the pump frequency in radians per second. Differentiating Eq. (2) with respect to time we have the mean velocity

for the oscillating flow

$$u = u_{max}\sin(\omega t) \tag{3}$$

The stroke frequency n (in strokes or cycles per second) then follows from:

$$n = \omega/(2\pi) \tag{4}$$

The average volume flow rate q_{av} is equal to the product of stroke volume and pump frequency [25]:

$$q_{av} = \omega/(2\pi)SA_p \tag{5}$$

The pressure gradient takes the form:

$$-\frac{1}{\rho}\frac{\partial p}{\partial x} = ae^{i\omega t} \tag{6}$$

The definition of the critical Reynolds number for the reciprocating flow in the main pipe is given by:

$$Re_{\omega} = \frac{\omega D^2}{v} = 354.32 \tag{7}$$

4.1.1. Flow characteristics for the reciprocating mechanism

Reynolds number in the pipe indicates that the flow in the pipe is turbulent. The velocity profile for the oscillating motion of the fluid in a pipe which is driven by a sinusoidal pressure gradient was integrated over the cross section of a pipe as given by Eq. (2) and simplified for the Reynolds number range covering the value obtained in Eq. (6) [22,26]:

$$\overline{V} = \frac{V_{max}}{\tau R}\int_0^R\int_0^{\tau}\left(\frac{32}{r\sigma Re_{\omega}}\left[\sin t - \left(e^{-E}\right)\sin(t-E)\right]\right) \tag{8}$$

and

$$E = \left[1 - \left(\frac{r}{R}\right)^2\right]\sqrt{\frac{Re_{\omega}}{8}} \tag{9}$$

$$\sigma = \frac{8}{\alpha^3}\sqrt{(\alpha - 2C_1)^2 + 4C_2^2} \tag{10}$$

$$C_1 = \frac{ber\alpha bei'\alpha - bei\alpha ber'\alpha}{ber^2\alpha + bei^2\alpha} \tag{11}$$

$$C_2 = \frac{ber\alpha bei'\alpha + bei\alpha ber'\alpha}{ber^2\alpha + bei^2\alpha} \tag{12}$$

ber(), bei(), ber'() and *bei'()* are kelvin functions [27].

4.2. Governing equations

The formulation in the present study is based on the three-dimensional single phase equations of continuity, momentum, and energy under the conditions of, incompressible fluid, negligible dissipation and pressure work, constant fluid properties, and the Boussinesq approximation, along with appropriate boundary conditions, which require serious consideration because of the emphasis on reciprocating motion. And all the surfaces of the heat source exposed to the surroundings are assumed to be insulated except the interior walls of evaporator where constant heat flux simulates the heat generation from different components. Based on above assumptions, the governing equations for fluid and energy transport are:

$$\nabla\cdot\vec{V} = 0 \tag{13}$$

$$\frac{\rho\partial\left(\vec{V}\right)}{\partial t} + \rho\left(\vec{V}.\nabla\vec{V}\right) = -\nabla p + \mu\nabla^2\vec{V} \tag{14}$$

Energy in fluid flow

$$\rho c_p\frac{\rho D(T)}{Dt} = -k_s\nabla^2 T \tag{15}$$

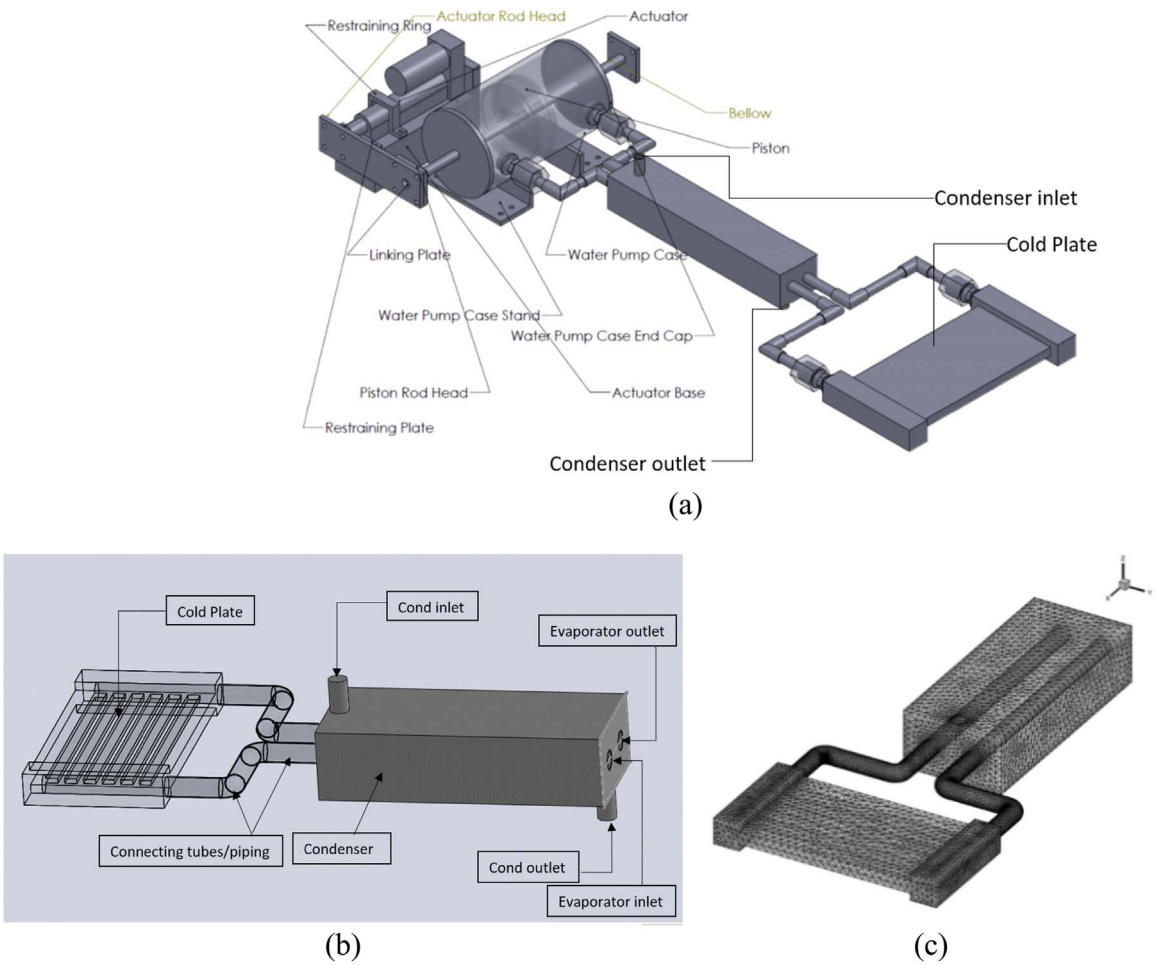

Fig. 3. (a) assembly diagram of RMDHL (b) geometry of the RMDH loop used for numerical model (c) grid distribution for the RMDH loop.

turbulent heat transport:

$$\rho\frac{\partial E}{\partial t} + \frac{\partial}{\partial t}\Big[V(\rho E + p)\Big] = k_s\nabla^2 T \tag{16}$$

The cold plate has an overall dimension of 5.91″ (15 cm) by 11.81″ (30 cm) with a maximum heat input of 550 W. Energy in heat sink solid part is modeled as

$$k_s(\nabla^2 T_s) = 0 \tag{17}$$

4.3. Turbulence modeling

The turbulence parameter are obtained from the following transport equations[28–39].

4.3.1. Standard k- ε Model

The turbulence kinetic energy (k) and turbulence rate of dissipation (ε) are given as follows:

$$\frac{\partial}{\partial t}(\rho k) + \frac{\partial}{\partial x_i}(\rho k u_i) = \frac{\partial}{\partial x_j}\left[\left(\mu + \frac{\mu_t}{\sigma_k t}\right)\frac{\partial k}{\partial x_j}\right] + G_k + G_b - \rho\varepsilon - Y_M + S_k \tag{18}$$

$$\frac{\partial}{\partial t}(\rho \varepsilon) + \frac{\partial}{\partial x_i}(\rho \varepsilon u_i) = \frac{\partial}{\partial x_j}\left[\left(\mu + \frac{\mu_t}{\sigma_\varepsilon t}\right)\frac{\partial \varepsilon}{\partial x_j}\right] + C_{1\varepsilon}\frac{\varepsilon}{k}(G_k + C_{3\varepsilon}G_b) - C_{2\varepsilon}\rho\frac{\varepsilon^2}{k} + S_\varepsilon \tag{19}$$

In these equations, G_k represents the generation of turbulence kinetic energy due to the mean velocity gradients; G_b is the generation of turbulence kinetic energy due to buoyancy, G_k represents the contribution of the fluctuating dilatation in

compressible turbulence to the overall dissipation rate, and $C_{1\varepsilon}$, $C_{2\varepsilon}$, and $C_{3\varepsilon}$ are the related constants [30]. The value of $C_{1\varepsilon}$ and $C_{2\varepsilon}$ are set at 1.44 and 1.92. σ_k and $\sigma_\varepsilon$are the turbulent Prandtl numbers for k and ε respectively with values 1.0 and 1.3 respectively, $S_k$and S_ε are source terms which in this study are set to be zero. Additional information on value selection and modeling equations of $G_k G_b G_k$ and $C_{3\varepsilon}$ are presented in [31]. The turbulent viscosity μ_t is modeled as follows:

$$\mu_t = \rho C_\mu \frac{k^2}{\varepsilon} \tag{20}$$

and C_μ is set at 0.09 [30,31].

4.3.2. RNG k- ε Model

The RNG k- ε Model is a modification of the standard k- ε Model. It includes additional term in its ε equation, incorporating the effect of swirl on turbulence, an analytical formula for turbulent Prandtl numbers and an analytically derived differential formula for effective viscosity. In addition to the documented swirl modification, additional modifications are shown in the following formulations [32]:

(i) $\left(\mu + \frac{\mu_t}{\sigma_k t}\right)$in Eq. (18) is substituted with $\alpha_k . \mu_{eff}$
(ii) $\left(\mu + \frac{\mu_t}{\sigma_\varepsilon t}\right)$in Eq. (19) is substituted with $\alpha_\varepsilon . \mu_{eff}$
(iii) Additional $-R_\varepsilon$in Eq. (18)
(iv) C_μ,$C_{1\varepsilon}$and $C_{2\varepsilon}$ is set at 0.0845,1.42 and 1.68, respectively.

α_k and α_ε are the inverse effective Prandtl number for k and ε respectively, and μ_{eff} is the effective viscosity [32].

4.3.3. Realizable k- ε Model

The Realizable k- ε Model is also a modification of the standard k- ε Model. It uses the same formulation for the k but has an alternative formulation for ε, Eq. (20) [33]:

$$\frac{\partial}{\partial t}(\rho\varepsilon) + \frac{\partial}{\partial x_i}(\rho\varepsilon u_i) = \frac{\partial}{\partial x_j}\left[\left(\mu + \frac{\mu_t}{\sigma_\varepsilon t}\right)\frac{\partial \varepsilon}{\partial x_j}\right] + \rho C_1 S\varepsilon + C_{1\varepsilon}\frac{\varepsilon}{k}_k . C_{3\varepsilon} G_b - \rho C_2 \frac{\varepsilon^2}{k + \sqrt{\nu\varepsilon}} + S_\varepsilon \tag{21}$$

where C_1 and C_2 are constants [33].

4.3.4. Standard k- ω

The transport equations for k and the specific dissipation rate (ω) are as follows [34]:

$$\frac{\partial}{\partial t}(\rho k) + \frac{\partial}{\partial x_i}(\rho k u_i) = \frac{\partial}{\partial x_j}\left[\Gamma_k \frac{\partial k}{\partial x_j}\right] + G_k - Y_k + S_k \tag{22}$$

$$\frac{\partial}{\partial t}(\rho\omega) + \frac{\partial}{\partial x_i}(\rho\omega u_i) = \frac{\partial}{\partial x_j}\left[\Gamma_\omega \frac{\partial \omega}{\partial x_j}\right] + G_\omega + Y_\omega + S_\omega \tag{23}$$

In these equations, G_k represents the generation of turbulence kinetic energy due to the mean velocity gradients, G_ω represents the generation of ω, Γ_k and Γ_ω represent the effective diffusivity of k and ω respectively, Y_k and Y_ω represent the dissipation of k and ω due to turbulence. All of the preceding terms are calculated and specified in [30,34].

4.3.5. Shear-stress transport (SST) k - ω Model

The SST k- ω model is a modification of the standard k- ω model. The modifications are as follows [35]:

(i) G_k in Eq. (22) is substituted with $\tilde{G}_k$
(ii) Additional D_ω is added to Eq. (23)

G_k represents the generation of turbulence kinetic energy due to mean velocity gradients, calculated from G_k and D_ω represents the cross-diffusion term [30,35], S_k and S_ω are source terms which in this study are set to be zero.

4.3.6. Transition k -k_L-ω

For an incompressible single-phase flow with no body forces, governed by the steady Reynolds-averaged continuity and momentum equations, and a linear eddy-viscosity model for the Reynolds stresses, the k -k_L-ω governing equations for turbulent kinetic energy k the laminar kinetic energy k_L, and the scale-determining variable ω are as follows [36]:

$$\frac{Dk}{Dt} = P_k + R_{BP} + R_{NAT} - \omega k - D_T + \frac{\partial}{\partial x_j}\left[\left(\upsilon + \frac{\alpha_T}{\alpha_k}\right)\frac{\partial k}{\partial x_j}\right] \tag{24}$$

$$\frac{Dk_L}{Dt} = P_{kL} + R_{BP} + R_{NAT} - \omega k - D_L + \frac{\partial}{\partial x_j}\left[\upsilon\frac{\partial k_L}{\partial x_j}\right] \tag{25}$$

$$\frac{D\omega}{Dt} = C_{\omega l}\frac{\omega}{k}P_k + \left(\frac{C_{\omega R}}{f_W} - 1\right)\frac{\omega}{k}(R_{BP} + R_{NAT}) - C_{\omega 2}\omega^2 + C_{\omega 3}f_\omega\alpha_T f_W^2\frac{\sqrt{k}}{d^3} + \left[\left(\upsilon + \frac{\alpha_T}{\sigma_\omega}\right)\frac{\partial\omega}{\partial x_j}\right] \tag{26}$$

The various terms in the model equations represent production, destruction, and transport mechanisms [29,36].

4.3.7. Transition SST model

The transition SST model is based on the coupling of the SST k- ω model with two other transport equations, one for the intermittency and one for the transition onset criteria, in terms of momentum-thickness Reynolds number. The transport equation for the intermittency$\gamma$and the various terms in the model equations representing production, destruction, and transport mechanisms are provided in [37–39].

4.4. Boundary conditions

The formulation in the conjugate heat transfer in the present study is based on the three-dimensional single -phase equations of continuity, momentum, and energy under the conditions of, incompressible fluid, negligible dissipation and pressure work, constant fluid properties, along with appropriate boundary conditions, which require serious consideration because of the emphasis on reciprocating motion. Applied boundary conditions are given as follows:

Inlet:

$$V = V_{in}, \qquad T_{in} = \left(T_{out}\right)_{ave} \tag{27}$$

Outlet:

$$P = P_{out}, \qquad \frac{\partial T}{\partial n} = 0 \tag{28}$$

Fluid–solid interface:

$$\vec{V} = 0, \qquad T = T_s, \qquad -k_s\frac{\partial T_s}{\partial n} = -k\frac{\partial T}{\partial n} \tag{29}$$

At the top wall:

$$q_w = -k_s\frac{\partial T_s}{\partial n} \tag{30}$$

Details of the numerical solution scheme are presented in Table 2. The CFD numerical algorithm utilizes Pressure Implicit with Splitting of Operators (PISO) formulation for the solution of the Navier-Stokes and heat transport equations. Gradient discretization was Green-Gauss Node based, pressure discretization was second order while the momentum and energy discretization were second order upwind. The turbulent Kinetic Energy and turbulent dissipation were first order upwind using the k-ε turbulence model. Transient formulation was second order Implicit. Appropriate under relaxations were used to improve the numerical stability for all governing equations. The criteria for convergence was set at 10^{-4} for the continuity equation, x, y and z momentum equations, and turbulent kinetic energy and turbulence dissipation equations.

5. Results

The current analysis is an open loop configuration for the reciprocating loop. The open loop configuration is achieved using a C++ code which closes the loop by transferring average flow conditions at the outlet of the loop to the inlet for the forward motion and vice versa for the reverse flow conditions. The loop assuming adiabatic, isochoric and isobaric conditions. In the forward direction the Boundary conditions for the inlet remains a velocity inlet and in the reverse flow the boundary condition reverses to a velocity outlet. The Virtual loop was implemented to reduce computational costs associated with fluid structure interaction required in modeling the pump.

The Mesh Information for Numerical investigation is shown in Table 1, the resulting computational mesh is presented in Fig. 3c. Numerical values for the boundary conditions is provided in Table 2. In order to establish computational accuracy, grid independence studies are always necessary and were equally performed in this work. A time-step of 0.005 was adopted for the study and given that convergence was achieved after an average of sixty thousand iterations, the average total flow time was 300 s. The mesh independence studies were conducted for two more Grids with coarse and fine meshes settings in ANSYS Fluent. With respect to temperature variation on the plate surface, the variation of the results between the coarsest

and finest meshes was 2% while the results showed less than 1.5% change for the last two grid size. The criteria for convergence was set at 10^{-4} for the continuity, *x*, *y* and *z* momentum, turbulent kinetic energy and turbulence dissipation rate. While a convergence criterion of energy was set at 10^{-7}.

The flow channel for the experimental and numerical setup of this conjugate heat transfer study consists of rectangular channels at the heat addition site within the cold plate and circular channel in the connecting pipping of the condenser section where heat removal occurs. The focus of the study is on the characteristic of the convection and conduction in the rectangular channel with constant heat flux. The boundary conditions as listed in Section 4 are One-dimensional, developing and fully developed steady heat transfer with constant thermal conductivity.

The effectiveness of the virtual loop is demonstrated when the results of this analysis is compared with similar works. The result of the velocity profile is very similar to the results obtained by [26,40] Fig. 4a is the velocity profile obtained for a two dimensional flow study by [26] and Fig. 4b is the result of the velocity profile for the y-z plane of the 3 dimensional flow in this study. In agreement with [40], the velocity profile has different shapes at accelerating half and decelerating half periods. The velocity is relatively steeper near the wall and flat towards the center. The average velocity shown in Fig. 5 has a parabolic definition along the channel.

Temperature variation on cold plate for all the solutions is typical of the results of single phase RMDHL cooling systems [24,41]. The temperature uniformity across the cold plate is such that the temperature is lower at the edges and gradually increases through the middle. This variation is different from conventional cooling using dynamic pumping system where the temperature will progressively increase from the coolant.

inlet to the outlet. Based on a time step of 0.005 adopted for the current study, the results of the numerical analysis indicate that the scatter between the numerical model is about 2 K. The temperature range across the cold plate is within 3 °C. *k*- ε models however produces a higher temperature uniformity across the cold plate than those of the *k*-ω based models. The comparism of the results of the numerical model to the data collected experimentally was done both graphically and statistically.

Addition visual comparism for the results of the turbulence based numerical model was carried using a consistent prost-processing setting, as shown in Fig. 6a–d. The figures show the temperature gradients as expected in such numerical analysis, which is that heat enters the system from the cold plate (evaporator) and the heat is removed from the system at the condenser, in terms of the contour of varying temperature across evaporator for varying heat transfer rate and varying stage in the numerical simulation. From Fig. 6 it is obvious that the results of the numerical models vary significantly for the cold plate (evaporator), condenser and the cooling fluid in the RMDHL loop. Fig. 7 is an x-y plot of the numerical results from different turbulence models as compared with the corresponding temperature measurement at each thermocouple location. From the results of Fig. 6, Figs. 7 and 8, it can be seen that some models such as RNG k-ε and Standard k-ε match the experimental data much better than others. However, additional investigation is needed to more accurately quantify the performance of each numerical model.

To standardize the results of this work and provide empirical basis for the results of this study to be benchmarked against other works, a numerical model calibration template [42] is adopted for comparing and ranking numerical model predictions for the cold plate temperature with measured data. The template investigates the accuracy of each numerical prediction and then bench marks each numerical result against data. The template adopts *y*-intercept of the best-fit regression (Pearson's correlation coefficient (r) and coefficient of determination (R^2), the Nash-Sutcliffe efficiency (NSE) presented in Eq. (31), the percentage bias (PBIAS) presented in Eq. (32) and RMSE-observations standard deviation ratio (RSR) presented in Eq. (33).

NSE determines the relative magnitude of the residual variance (“noise”) compared to the measured data variance (“information”) and is the best objective function for reflecting the overall fit hydrodynamics. NSE ranges between -∞ and 1.0, the closer NSE is to 1, the more accurate the prediction. PBIAS measures the average tendency of the simulated data to be larger or smaller than the experimental data, the lower the magnitude the more accurate the model simulation, and the optimal value would therefore be zero. RSR measures the error index and like the PBIAS, its optimal value is zero. A summary of the statistical analysis is presented in Table 3. From the template all the models appropriately reproduce the magnitudes of measured data. However, there are a few variations.

$$NSE = 1 - \frac{\sum_{i=1}^{n}\left(Y_i^{exp} - Y_i^{sim}\right)^2}{\sum_{i=1}^{n}\left(Y_i^{exp} - Y_i^{mean}\right)^2} \tag{31}$$

Table 1
Mesh information for numerical investigation.

Domain	Nodes	Tetrahedron elements	Total elements
body part	46,978	167,499	167,499
condenser part	88,243	165,196	275,326
evaporate part	129,837	149,526	338,421
All Domains	265,059	482,221	781,246

Table 2
Boundary conditions for the present simulation.

Boundary conditions	**Values and their range**	
Inlet velocity of the evaporator	varying stroke (cm)	7.62,
	frequency (n)	0.14
Inlet velocity of the condenser	1.223 m/s	
Inlet temperature of the condenser	283 K	
Solid wall thickness	0.0001 m	
Heat (Q)	**Heat (W)**	**Average heat flux (W/m^2)**
	606.00	8,780.16
	558.00	8,084.70
	505.00	7,316.80
	464.00	6,722.77

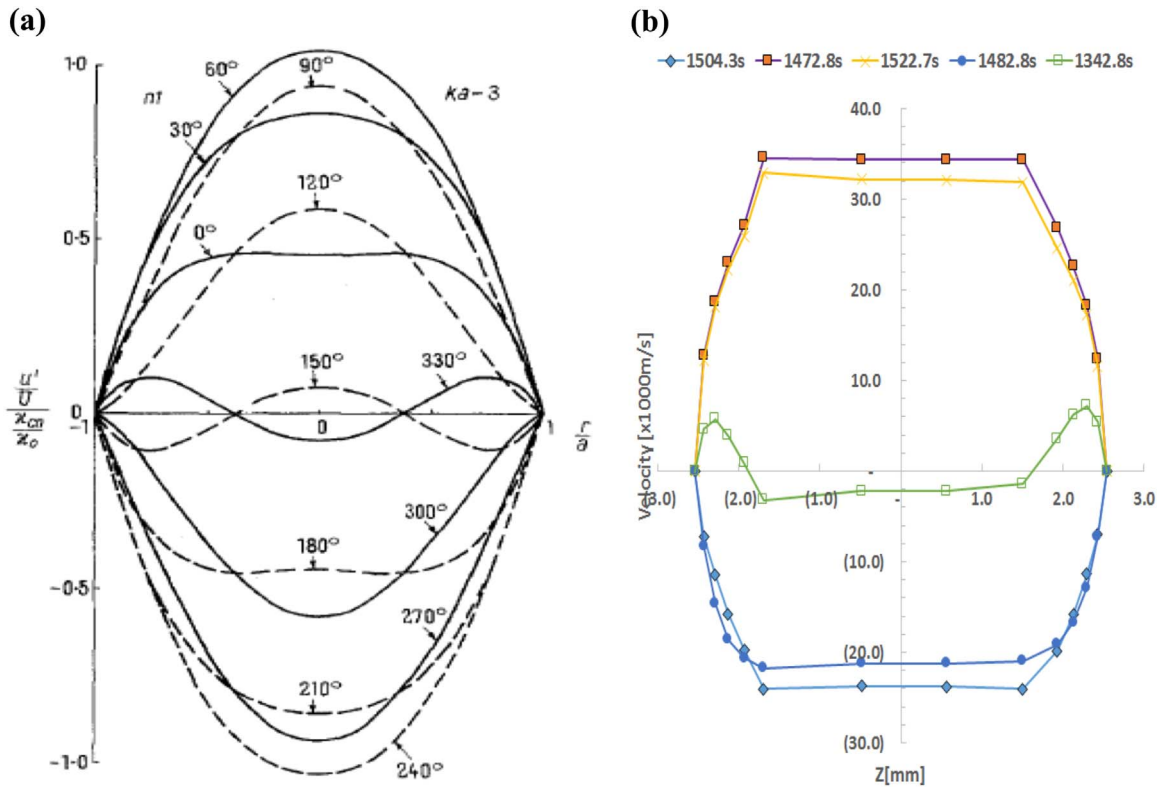

Fig. 4. Velocity profile for (a) pulsating viscous flow [26] (b) pulsating viscous flow for this study at various times.

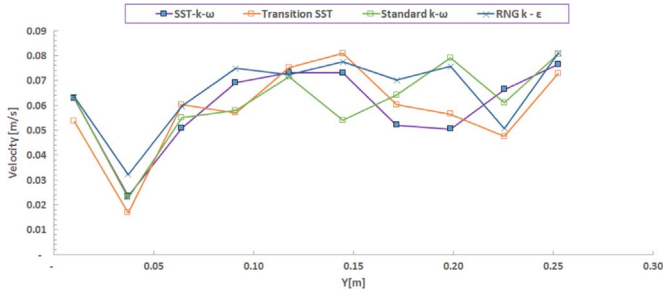

Fig. 5. Average velocity variation along rectangular flow channel in the cold plate.

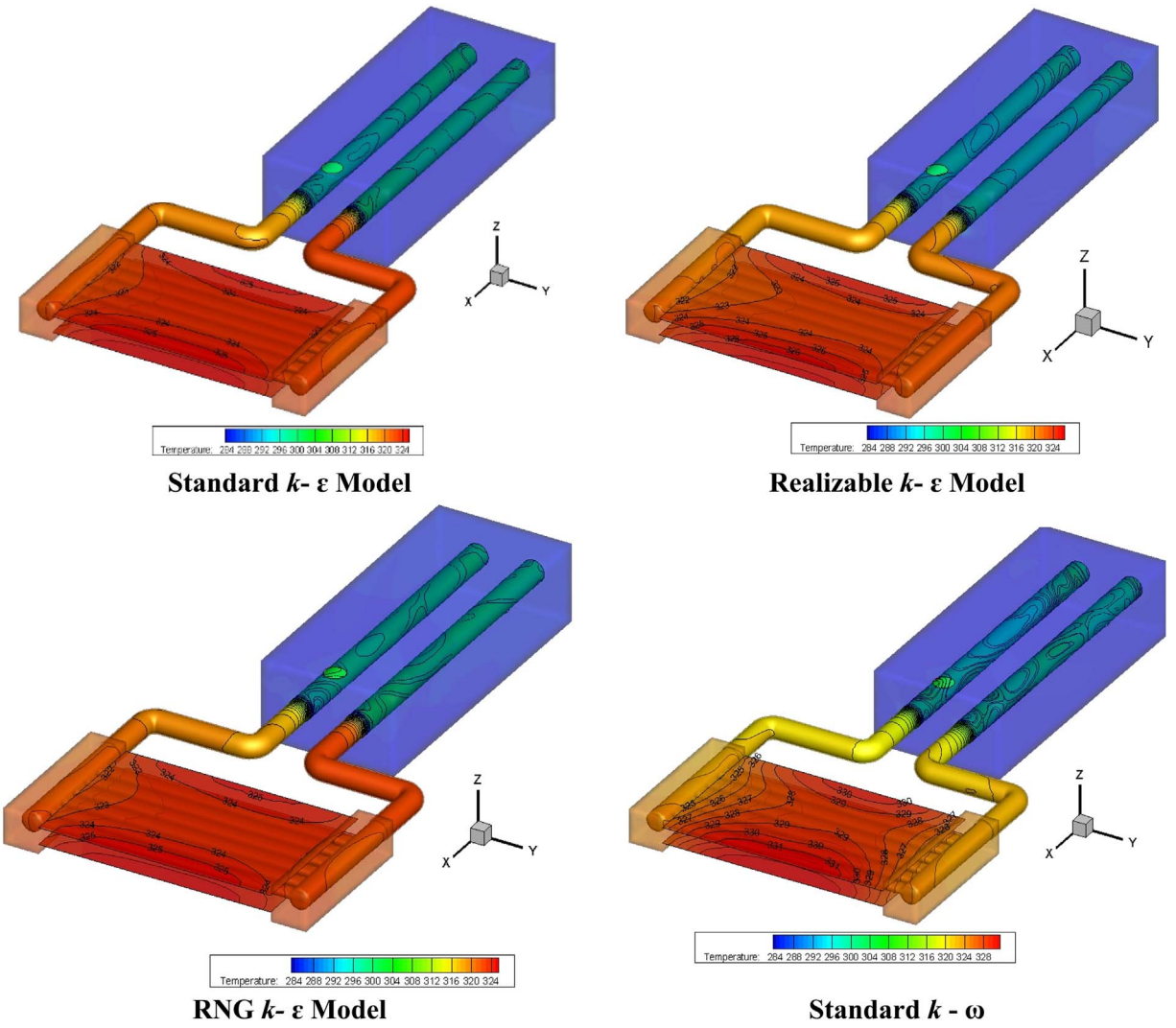

Fig. 6. Temperature contours of RMDHL assembly model for various turbulence prediction model.

$$PBIAS = \frac{\sum_{i=1}^{n}\left(Y_i^{exp} - Y_i^{sim}\right) \times (100)}{\sum_{i=1}^{n}\left(Y_i^{exp}\right)} \tag{32}$$

$$RSR = \frac{\sqrt{\sum_{i=1}^{n}\left(Y_i^{exp} - Y_i^{sim}\right)^2}}{\sqrt{\sum_{i=1}^{n}\left(Y_i^{exp} - Y_i^{mean}\right)^2}} \tag{33}$$

In terms of computational time, the average number of iterations for convergence for all the turbulence models averaged about 60k iterations, however the computational time for the standard k- ε models standard k-ω were significantly lower while the Transition k -k_L-ω was significantly higher than the other Models. This information may require when computational resources are scarce or in a system where the speed of the numerical analysis is factor to consider. A variation of heat input for the coolant was carried out as shown in Table 2 and Fig. 5a and b. For all numerical models considered the average cold plate temperature increased with increasing heat input however, based on the empirical statistical analysis using the template, the performance of the model is independent of heat input. Although this work did not investigate the effect on turbulence models on pressure drop, the value of the slope of the RNG k - ε may indicate that the pressure drop may be influence by the turbulence models. The value of the slope for the RNG k - ε model has a positive value whereas all the other models have a negative value. Incidentally, the slope of the experimental results also has a positive value.

The value of the slope for all turbulence models as well as the experimental data is within the range of ± 1. The slope indicates that all the results from all the turbulence models provide the measured experimental values are linearly related. From the y intercept and the slope values the data suggests that the RNG k - ε provides the best prediction for the magnitude

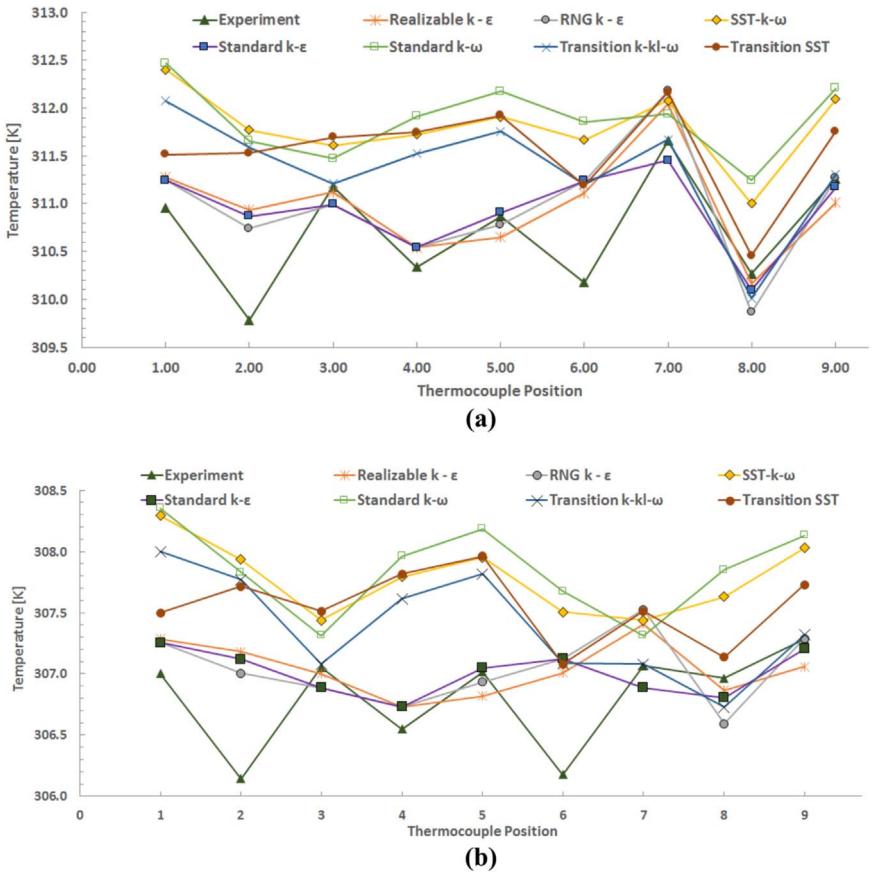

Fig. 7. Temperature distributions over the cold plate for experimental and the numerical models for (a)8.8 kW/m^2 (b)6.7 kW/m^2.

of average temperature of the measured data. The Slope indicates that the RNG k - ε also provides a better prediction of the linear variation in temperature across.

the cold plate surface. NSE, RSR and PBIAS for all the numerical models were less than ± 1, implying that all the turbulence models will provide strongly suitable correlations to the experimental results. This note is of importance to address the point raised in the introductions that correlation for oscillating flow are not explicitly developed as they are obtained from using correlations relating to continuous flow because in the correlations for modeling.

The PBIAS the show that the magnitude of the results for the numerical k-ω based models tend to be larger than the magnitude of the experimental data. Physical examination of the plots indicates that the k-ω models may provide a better prediction of the fluctuations in temperature. But the RSR values suggest that the k-ω Models contain more noise related values than the k- ε Model. This is of interest as traditionally, k-ω Models are preferred to the k- ε Model for internal flows. The reason for this may be associated with the k-ω Models contain a wall function as part of its formulation, and the sinusoidal variation of flow velocity and pressure may make the results of the k-ω Models less stable when compared to the results of the k- ε models. On the other hand, NSE indicates how well the plot of observed data fits the simulated data [42]. We can conclude that the RNG k- ε Model based models provide better magnitude predictions, collinearity to the measured data, and least noise. The standard k- ε model and the realizable k- ε Model and just as effective as standard k- ε models but the k-ω based models were the least accurate in magnitude prediction.

6. Conclusion

In order to improve the accuracy of CFD model for the RMDHL, extensive numerical simulations with different turbulence models have been carried out to study fully developed turbulent, low velocity and high heat reciprocating flow. The flow statistics obtained from the numerical results of seven selected turbulent prediction models and available measurement data have been compared, and in general a good agreement between the numerical simulation and experiment is obtained. The accuracy of the numerical models against the experimental data was also quantitatively analyzed. To identify the most accurate turbulence prediction model, template of Moriasi et al. [42], adopted. The results indicate that for a close prediction of the average cold plate temperature, the standard k- ε Model models provides the best accuracy while the RNG

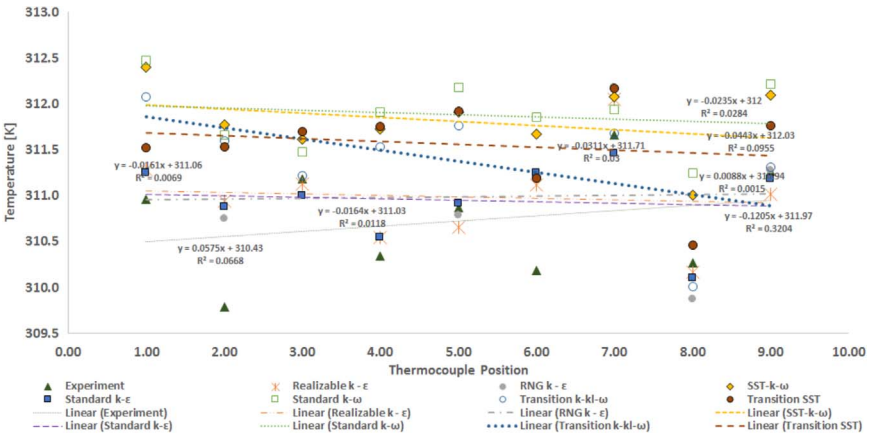

Fig. 8. *y*-intercept of the best-fit regression temperature distributions over the cold plate.

Table 3
Results for statistical and ranking for turbulent prediction methods.

Model		Experiment	Realizable *k* - ε	RNG *k* - ε	Standard *k*-ε	SST-*k*-ω	Standard *k*-ω	Transition *k* -k_L-ω	Transition SST
Regression	r		0.62	0.67	0.56	0.51	0.39	0.30	0.60
	R^2	0.067	0.007	0.001	0.019	0.096	0.028	0.320	0.030
	Slope	0.058	−0.016	0.009	−0.016	−0.044	−0.002	−0.121	−0.031
	Intercept	310.43	311.06	310.94	311.03	312.03	312.00	311.97	311.71
NSE			0.12	0.11	0.15	−3.31	−3.97	−1.63	−1.78
PBIAS			−0.08	−0.08	−0.07	−0.35	−0.37	−0.21	−0.27
RSR			0.94	0.94	0.92	2.08	2.23	1.62	1.67

k- ε Model provides more accurate information with respect to variations in temperature across the cold plate surface and will generally provide the best qualitative and quantitative basis for additional modeling consideration for future RMDHL study.

References

[1] Y. Cao, M. Gao, Experimental and analytical studies of reciprocating-mechanism driven heat loops (RMDHLs), J. Heat. Transf. (2008) 0729011–0729016.
[2] Y. Cao, D. Xu, M. Gao, Experimental study of a bellows-type reciprocating-mechanism driven heat loop, Int. J. Energy Res. 37 (6) (2013) 665–672.
[3] M.B. Ibrahim, Z. Zhang, R. Wei, A 2-D CFD model of oscillatory flow with jets impinging on a random wire regenerator matrix, Intersoc. Energy Convers. Eng. Conf. (2002) 1–7.
[4] M.B. Ibrahim, Z. Zhang, S. Kembhavi, A 2-D axisymmetric CFD model of oscillatory flow with separation, in: Proceedings of Energy Conversion Engineering Conference, 2002. IECEC '02. 2002 37th Intersociety, vol. 37, 2002, pp. 511–517.
[5] O. Popoola, A. Bamgbade, Y. Cao, A numerical model of a reciprocating-mechanism driven heat loop (RMDHL) for two-phase high heat flux cooling, J. Therm. Sci. Eng. Appl. (2016) 1–20.
[6] M. Nallasamy, Turbulence models and their applications to the prediction of internal flows: a review, Comput. Fluids 15 (2) (1987) 151–194.
[7] N.C. Markatos, The mathematical modelling of turbulent flows, Appl. Math. Model. 10 (3) (1986) 190–220.
[8] M. Gundogdu, M. Carpinlioglu, Present state of art on pulsatile flow theory: Part 1: laminar and transitional flow regimes, JSME Int. J. Ser. B Fluids Therm. Eng. 42 (3) (1999) 384–397.
[9] M.Y. Gündoğdu, M.Ö. Çarpınlıoğlu, Present state of art on pulsatile flow theory, part 2. Turbulent flow regime, JSME Int. J. Ser. B Fluids Therm. Eng. 42 (3) (1999) 398–410.
[10] M. ÖzdinçÇarpinlioğlu, M. Yaşar Gündoğdu, A critical review on pulsatile pipe flow studies directing towards future research topics, Flow Meas. Instrum. 12 (3) (. 2001) 163–174.
[11] K.H. Ahn, M.B. Ibrahim, A 2-D oscillating flow analysis in Stirling engine heat exchangers, in: Proceedings of the 1991 Joint ASME-JSME Fluids Engineering Conference, 1991, pp. 159–164.
[12] M. Ibrahim, W. Hashim, Oscillating flow in channels with a sudden change in cross section, Comput. Fluids 23 (1) (1994) 211–224.
[13] Y. Su, J.H. Davidson, F.A. Kulacki, Numerical investigation of fluid flow and heat transfer of oscillating pipe flows, Int. J. Therm. Sci. 54 (2012) 199–208.
[14] K. Versteeg, H. Malalasekera, An introduction to computational fluid dynamics: the finite volume method, vol. M., Pearson, Essex, 2007.
[15] M. Ghafarian, D. Mohebbi-Kalhori, J. Sadegi, Analysis of heat transfer in oscillating flow through a channel filled with metal foam using computational fluid dynamics, Int. J. Therm. Sci. 66 (2013) 42–50.
[16] L. Wang, X.-Y. Lu, An investigation of turbulent oscillatory heat transfer in channel flows by large eddy simulation, Int. J. Heat. Mass Transf. 47 (10–11) (2004) 2161–2172.
[17] T. Zhao, P. Cheng, A numerical solution of laminar forced convection in a heated pipe subjected to a reciprocating flow, Int. J. Heat Mass Transf. 38 (16) (1995) 3011–3022.
[18] C. Sert, A. Beskok, Numerical simulation of reciprocating flow forced convection in two-dimensional channels, J. Heat. Transf. 125 (2003) 403–412.
[19] B.L. Jensen, B.M. Sumer, J. Fredsoe, Turbulent oscillatory boundary layers at high Reynolds numbers, J. Fluid Mech. 206 (1) (1989) 265–297.
[20] C. Walther, H.-D. Kühl, S. Schulz, Numerical investigations on the heat transfer in turbulent oscillating pipe flow, Heat. Mass Transf. 36 (2) (2000) 135–141.

[21] D.-Y. Lee, S.-J. Park, S. Tack Ro, Heat transfer in the thermally developing region of a laminar oscillating pipe flow, Cryogenics 38 (6) (1998) 585–594.
[22] T.S. Zhao, P. Cheng, Heat transfer in oscillatory flows, in: C.L. Tien (Ed.), Annual Review of Heat Transfer, IX, Begell House Inc., 1998, pp. 359–419.
[23] T.S. Zhao, P. Cheng, The friction coefficient of a fully-developed laminar reciprocating flow in a circular pipe, Int. J. Heat Fluid Flow 17 (96) (1996) 167–172.
[24] O.T. Popoola, Y. Cao, Application of a reciprocatory driven heat loop to high heat single phase liquid cooling for temperature uniformity, in: Proceedings of the OAU Faculty of Technology Conference (OAU TekCONF 2015), 2015, pp. 28–37.
[25] J. De-Jongh, R. Rijs (Eds.), Pump Design, Arrakis, Veldhoven, 2004.
[26] S. Uchida, The pulsating viscous flow superposed on the steady laminar motion of incompressible fluid in a circular pipe, Z. Angew. Math. Phys. ZAMP 7 (5) (1956) 403–422.
[27] M. Abramowitz, Irene A. Stegun, Handbook of Mathematical Functions, Dover, 1972.
[28] David C. Wilcox, Turbulence-Modeling-for-CFD, 3rd ed., DCW Industries, La Canada, CA, 2006.
[29] S.-E. Kim, D. Choudhury, B. Patel, Computations of complex turbulent flows using the commercial code fluent, in: M. Salas, J. Hefner, L. Sakell (Eds.), Modeling Complex Turbulent Flows SE − 15, 7, Springer, Netherlands, 1999, pp. 259–276.
[30] R.A.W.M. Henkes, F.F. Van Der Vlugt, C.J. Hoogendoorn, Natural-convection flow in a square cavity calculated with low-Reynolds-number turbulence models, Int. J. Heat. Mass Transf. 34 (2) (1991) 377–388.
[31] B.E. Launder, D.B. Spalding, The numerical computation of turbulent flows, Comput. Methods Appl. Mech. Eng. 3 (2) (1974) 269–289.
[32] V. Yakhot, L.M. Smith, The renormalization group, the ε-expansion and derivation of turbulence models, J. Sci. Comput. 7 (1) (1992) 35–61.
[33] T.H. Shih, W.W. Liou, A. Shabbir, Z. Yang, J. Zhu, A new K-epsilon eddy viscosity model for high Reynolds number turbulent flows: model development and validation, Comput. Fluids 24 (1995) 227–238.
[34] F.R. Menter, Turbulence modeling for engineering flow, Canonsburg, 2011.
[35] F.R. Menter, Two-equation eddy-viscosity turbulence models for engineering applications, AIAA J. 32 (8) (1994) 1598–1605.
[36] D.K. Walters, D. Cokljat, A three-equation eddy-viscosity model for Reynolds-averaged Navier–Stokes simulations of transitional flow (121401–1–14), J. Fluids Eng. 130 (12) .
[37] R.B. Langtry, F.R. Menter, S.R. Likki, Y.B. Suzen, P.G. Huang, S. Völker, A correlation-based transition model using local variables—part II: test cases and industrial applications, J. Turbomach. 128 (3) (2006) 423–434.
[38] F.R. Menter, R.B. Langtry, S.R. Likki, Y.B. Suzen, P.G. Huang, S. Völker, A correlation-based transition model using local variables—part I: model formulation, J. Turbomach. 128 (3) (2006) 413–422.
[39] R. Langtry, F. Menter, Transition modeling for general CFD applications in aeronautics, in: Proceedings of the 43rd AIAA Aerospace Sciences Meeting and Exhibit, American Institute of Aeronautics and Astronautics, 2005.
[40] T.S. Zhao, P. Cheng, A numerical study of laminar reciprocating flow in a pipe of finite length, Appl. Sci. Res. 59 (1998) 11–25.
[41] O.T. Popoola, S. Soleimanikutanaei, Y. Cao, Reciprocating-mechanism driven heat loop (RMDHL) cooling technology for power electronic systems, in: S. M.S. Murshed (Ed.), Electronic Cooling, Intech, Rijeka, Croatia, 2016.
[42] D.N. Moriasi, J.G. Arnold, M.W. Van Liew, R.L. Binger, R.D. Harmel, T.L. Veith, Model evaluation guidelines for systematic quantification of accuracy in watershed simulations, Trans. ASABE 50 (3) (2007) 885–900.